The Relative Stability Against Merger of Close, Compact Binaries

Kimberly C. B. New¹ and Joel E. Tohline Department of Physics & Astronomy, Louisiana State University, Baton Rouge, LA 70803-4001

ABSTRACT

The orbital separation of compact binary stars will shrink with time due to the emission of gravitational radiation. This inspiralling phase of a binary system's evolution generally will be very long compared to the system's orbital period, but the final coalescence may be dynamical and driven to a large degree by hydrodynamic effects, particularly if there is a critical separation at which the system becomes dynamically unstable toward merger. Indeed, if weakly relativistic systems (such as white dwarf–white dwarf binaries) encounter a point of dynamical instability at some critically close separation, coalescence may be entirely a classical, hydrodynamic process. Therefore, a proper investigation of this stage of binary evolution must include three–dimensional hydrodynamic simulations.

We have constructed equilibrium sequences of synchronously rotating, equal-mass binaries in circular orbit with a single parameter – the binary separation – varying along each sequence. Sequences have been constructed with various polytropic as well as realistic white dwarf and neutron star equations of state. Using a Newtonian, finite-difference hydrodynamics code, we have examined the dynamical stability of individual models along these equilibrium sequences. Our simulations indicate that no points of instability exist on the sequences we analyzed that had relatively soft equations of state (polytropic sequences with polytropic index n = 1.0 and 1.5 and two white dwarf sequences). However, we did identify dynamically unstable binary models on sequences with stiffer equations of state (n = 0.5 polytropic sequence and)two neutron star sequences). We thus infer that binary systems with soft equations of state are not driven to merger by a dynamical instability. For the n = 0.5 polytropic sequence, the separation at which a dynamical instability sets in appears to be associated with the minimum energy and angular momentum configuration along the sequence. Our simulations suggest but do not conclusively demonstrate that, in the absence of relativistic effects, this same association may also hold for binary neutron star systems.

Subject headings: binaries: close — hydrodynamics — instabilities — stars: neutron — white dwarfs

¹Currently at the Department of Physics & Atmospheric Science, Drexel University, Philadelphia, PA 19104

1. Introduction

The coalescence of double white dwarf and double neutron star binaries is important to examine since this process may produce a number of astrophysically interesting objects and events. Double white dwarf binary mergers have been suggested as precursors to some Type Ia Supernovae (Iben & Tutukov 1984; Iben 1988, 1991; Iben & Webbink 1989; Branch et al. 1995) and to long gamma-ray bursts (Katz & Canel 1996). White dwarf-white dwarf mergers may also lead to the formation of massive single white dwarfs or neutron stars (Colgate & Petschek 1982; Saio & Nomoto 1985; Iben & Tutukov 1986; Kawai, Saio, & Nomoto 1987; Chen & Leonard 1993); to the formation of subdwarf stars; or to the formation of hydrogen deficient, highly luminous stars (Iben 1990 and references therein; Webbink 1984). Neutron star-neutron star mergers may result in bursts of gamma-rays and neutrinos, in the production of r-process elements, and in the formation of black holes (Eichler et al. 1989; Meyer 1989; Narayan, Paczński, & Piran 1992; Rasio & Shapiro 1992; Davies, Benz, Piran, & Thielemann 1994; Katz & Canel 1996; Lipunov et al. 1995; Ruffert, Janka, & Schäfer 1996; but see the simulations of Shibata, Nakamura, and Oohara [1993] and Janka & Ruffert [1996] which cast doubt on the neutron star-neutron star merger scenario as a precursor to gamma-ray bursts).

Merging compact binaries are also expected to be relatively strong sources of gravitational radiation. The gravitational radiation emitted during the inspiral phase of double neutron star binary evolution (i.e., before tidal effects become sizeable) is likely to be detected by terrestrial interferometric detectors such as LIGO and VIRGO, which will be sensitive to frequencies in the range of $10-10^3$ Hz (Abramovici et al. 1992; Cutler et al. 1993; Thorne 1995). Proposed "dual-recycled" interferometers and spherical "TIGA" type resonant detectors will be more sensitive than LIGO to the higher frequency radiation, $\gtrsim 10^3$ Hz, emitted during the brief final merger stage of the coalescence (Meers 1988; Strain & Meers 1991; Cutler et al. 1993; Merkowitz & Johnson 1994; Thorne 1995; however, see Wilson & Mathews 1995 who indicate that the gravitational wave radiation emitted during this phase may have a lower frequency than previously expected). The gravitational wave radiation emitted during the merger phase in double white dwarf binary evolution is unlikely to be detected in the near future because the expected frequency of the radiation falls in or just beyond the upper end of the frequency range $(10^{-4}-10^{-1} \text{ Hz})$ of proposed space-based laser interferometric detectors (Faller et al. 1989; Hough et al. 1995) and the duration of the phase will be too short to produce a significant signal in this range of the detectors' sensitivity.

Because the final stages of binary coalescence are driven in part by sizeable nonlinear tidal effects, numerical hydrodynamic techniques must be used to properly follow the evolution of merging binaries. The first step in performing such a hydrodynamic simulation is the construction of an appropriate initial model. The coalescence of the chosen binary system must proceed on a dynamical timescale (on the order of a few initial orbital periods), in order for an explicit hydrodynamics code to be able to carry out the simulation in a reasonable amount of computational time. Hence, the components of the initial binary model must either be at a separation where they

are dynamically unstable to coalescence or they must be forcibly brought to coalescence from a wide separation (e.g., by draining orbital angular momentum away from the system in a way that mimics the effects of the gravitational wave radiation reaction). Using the former methodology, the work presented herein focuses on the identification of dynamically unstable binary systems.

The initial separation at which a particular binary model becomes dynamically unstable to merger, if one exists, can be found via a stability analysis of a set of binary models constructed in hydrostatic equilibrium, along a constant mass sequence of decreasing orbital separation. This sequence serves as an approximate representation of the evolution of the binary as its components are brought closer together by the effects of gravitational radiation. Such analyses have recently been done by Lai, Rasio, & Shapiro (hereafter LRS) and by Rasio & Shapiro (hereafter RS) for binaries with polytropic equations of state (EOS). In a polytropic equation of state, the pressure P is expressed in terms of the density ρ as $P = K \rho^{1+1/n}$, where K is the polytropic constant and n is the polytropic index (see §2). The analytical work of LRS utilized an approximate energy variational method and studied detached binaries with components having various mass ratios, spins, and polytropic indices (LRS 1993a, b, 1994a, b). The numerical work of RS utilized the smoothed particle hydrodynamics technique to study detached and contact binaries with components having various mass ratios, but equal spins and polytropic indices (RS 1992, 1994, 1995; for earlier work see Gingold & Monaghan 1979; Hachisu & Eriguchi 1984a, b; Hachisu 1986b).

We performed stability analyses of equilibrium sequences of double white dwarf binaries constructed with the zero-temperature white dwarf equation of state (Chandrasekhar 1967), double neutron star binaries constructed with realistic neutron star equations of state (adapted from Cook, Shapiro, & Teukolsky 1994), and, for the sake of comparison with the work of LRS and RS, polytropic binaries with n = 0.5, 1.0, and 1.5 equations of state. The examined equilibrium sequences were constructed with the Self-Consistent Field technique of Hachisu (1986a, b), which produces models of rotating, self-gravitating fluid systems in hydrostatic equilibrium. For simplicity, all binary models along these sequences were constructed as synchronously rotating systems having equal-mass (q = 1.0) components. The relative stability of individual binary systems along selected sequences was examined using a three-dimensional (3D), finite-difference hydrodynamics code. Both the construction of our equilibrium binary sequences and our stability tests along these sequences have been done using purely Newtonian gravity and Newtonian dynamics.

Our numerical techniques are briefly described in Section 2. Constructed equilibrium sequences are presented in Section 3 and our dynamical tests of the stability of individual models along selected sequences are presented in Section 4. Finally, the implications of these results are discussed in Section 5.

2. Numerical Techniques

Our simulations of close binary systems involve the solution of the following set of equations which govern the structure and evolution of a nonrelativistic fluid in cylindrical coordinates: the continuity equation,

$$\frac{\partial \rho}{\partial t} + \nabla \cdot (\rho \vec{v}) = 0; \tag{1}$$

the three components of the equation of motion,

$$\frac{\partial S}{\partial t} + \nabla \cdot (S\vec{v}) = -\frac{\partial P}{\partial R} - \rho \frac{\partial \Phi}{\partial R} + \frac{A^2}{\rho R^3},\tag{2}$$

$$\frac{\partial \mathcal{T}}{\partial t} + \nabla \cdot (\mathcal{T}\vec{v}) = -\frac{\partial P}{\partial z} - \rho \frac{\partial \Phi}{\partial z}, \qquad (3)$$

$$\frac{\partial A}{\partial t} + \nabla \cdot (A\vec{v}) = -\frac{\partial P}{\partial \phi} - \rho \frac{\partial \Phi}{\partial \phi}; \tag{4}$$

Poisson's equation

$$\nabla^2 \Phi = 4\pi G\rho; \tag{5}$$

and the equation of state (see below). In the above equations, \vec{v} is the velocity; $S = \rho u$, $\mathcal{T} = \rho w$, and $A = \rho R v_{\phi}$ are the radial, vertical, and angular momentum densities, respectively (where u, w, and v_{ϕ} are the radial, vertical, and azimuthal components of the velocity, respectively); R, ϕ , and z are the cylindrical coordinates; and Φ is the gravitational potential.

We have used three types of barotropic equations of state in this work. The first, and simplest, type is a polytropic equation of state for which

$$P = K\rho^{1+1/n},\tag{6}$$

where K is the polytropic constant and n, the polytropic index, determines the degree of compressibility of the fluid (the higher the value of n, the more compressible/softer the fluid).

The second type of equation of state used is the zero–temperature white dwarf (WD) equation of state (Chandrasekhar 1967), which represents the pressure distribution of a completely degenerate electron gas:

$$P = a_0 \left[x \left(2x^2 - 3 \right) \left(x^2 + 1 \right)^{1/2} + 3 \ln \left(x + \sqrt{1 + x^2} \right) \right]$$

$$x \equiv (\rho/b_0)^{1/3},$$
(7)

where $a_0 = 6.00 \times 10^{22}$ dynes cm⁻², $b_0 = 1.95(\mu_e/2) \times 10^6$ g cm⁻³, and μ_e is the mean molecular weight per electron. We have used $\mu_e = 2$ in all of our computations. The heaviest nonrotating single object that can be constructed with this equation of state has a mass of $1.44M_{\odot}$ (this is the Chandrasekhar mass M_{CH}).

The third type of equation of state used here is a realistic neutron star (NS) equation of state. We have chosen three such equations of state (from among the fourteen realistic NS equations of state listed in Cook, Shapiro, & Teukolsky [1994, hereafter CST]), each with a different degree of compressibility (one soft, one medium, and one hard). Specifically, the chosen soft equation of state is CST's equation of state F; the medium one is CST's equation of state FPS; and the hard one is CST's equation of state L (see references within CST for the original sources of these equations of state). We obtained these equations of state in tabular form from Cook (1995). The tables each provide ~ 500 values of the pressure P for values of ρ ranging over 15 orders of magnitude, from ~ 8 g cm⁻³ to 10^{16} g cm⁻³ (note that it is actually the number density $N = \rho/m_{neutron}$, where $m_{neutron} = 1.67 \times 10^{-24}$ g, that is tabulated). Because we wanted to perform *parallel* finite–difference hydrodynamics (FDH) simulations of systems with these equations of state and did not possess an interpolation algorithm designed for efficient use on a parallel machine, polynomial fits to the tabular data were necessary. Some numerical manipulation of the data was also needed because of the particulars of the technique used in the initial model construction. (See New [1996] for details.)

If the only motion of a fluid system is rotation about an axis with an angular velocity Ω , which is constant in time and a function only of the distance from the rotation axis, the structure of the system is described by the following single expression:

$$\frac{1}{\rho}\nabla P + \nabla\Phi + \nabla\Psi(R) = 0, \tag{8}$$

where the z-axis has been chosen as the axis of rotation and the centrifugal potential $\Psi(R) = -\int \Omega^2(R) R \, dR$. Such a fluid is said to be in hydrostatic equilibrium because the forces due to its pressure and to its gravitational and centrifugal potentials are in balance. All of the initial equilibrium binary systems studied in this work have been constructed in hydrostatic equilibrium according to this prescription, along with the additional constraint that angular velocity is a spatial constant Ω_0 (i.e., not a function of R). In this case of uniform rotation, $\Psi(R) = -\Omega_0^2 R^2/2$.

2.1. Self–Consistent Field Code

The method we have used to construct the equilibrium models is Hachisu's grid-based 3D, Self-Consistent Field (HSCF) technique (Hachisu 1986a, b). This iterative technique produces rotating, self-gravitating fluid systems in hydrostatic equilibrium. Our version of the HSCF 3D code computes the gravitational potential via a direct numerical solution of Poisson's equation (5). Details of the method used can be found in Tohline (1978).

An estimate of the quality of the converged equilibrium configuration is obtained from a determination of how well the energy is balanced in the system. This balance is measured by the

virial error VE:

$$VE \equiv \frac{\mid 2T + W + 3\int P \, dV \mid}{\mid W \mid},\tag{9}$$

where T is the kinetic energy; W is the gravitational potential energy; and V is the volume of the model. The virial errors in our equilibrium models constructed with polytropic and WD EOS were typically $\sim 10^{-3}$ - 10^{-4} ; those in models constructed with the realistic NS EOS were typically $\sim 10^{-2}$.

The forms of the WD and realistic NS equations of state are such that when they are used in the HSCF code, the density maxima ρ_{max} of the models to be constructed must be given to the code as input. Thus because we were interested in constant mass sequences for our stability analyses of close binaries, we had to perform an iteration in the choice of ρ_{max} until we arrived at a configuration with the desired M_T , in the case of models with the WD and realistic NS equations of state. However, in the polytropic case, converged models can actually be obtained without an *a priori* choice of ρ_{max} and then later scaled as desired.

Our 3D equilibrium configurations are assumed to be symmetric about the z = 0 (equatorial) plane; this symmetry will be referred to as equatorial symmetry. Because our version of the 3D HSCF code constructs binaries with only equal-mass components, a periodic symmetry over the azimuthal range $0 < \phi < \pi$ is also assumed. This means that a quantity U specified at an angle ϕ is equivalent to that same quantity specified at all angles ϕ' for which $\phi' = (\phi + m\pi)$ and m is an integer:

$$U(\phi + m\pi) = U(\phi). \tag{10}$$

This symmetry will be referred to as π -symmetry.

2.2. Finite–Difference Hydrodynamics Code

A finite-difference hydrodynamics (FDH) code was used to solve, on a discrete numerical grid, equations (1-5) and an equation of state (see above), which govern the temporal evolution of a fluid. FDH codes differ from smoothed particle hydrodynamics (SPH) codes in that they follow the evolution of the fluid as it flows through a fixed set of grid cells, instead of treating the fluid as a set of particles and following the evolution of each particle.

The 3D FDH code used in this present study is a Fortran 90 version of the Fortran 77 code described by Woodward (1992) and Woodward, Tohline, & Hachisu (1994). It was written, principally by Woodward, to take advantage of the parallel architecture of the MasPar computers on which it is run. The accuracy of the code is second order in both time and space. The numerical techniques employed are discussed in detail in Woodward (1992). The solution to Poisson's equation (5) is obtained through the ADI method (Cohl et al. 1997).

As in the HSCF code, the grid cells are uniformly spaced in each of the three directions and equatorial and π -symmetries are assumed. The single precision hydrodynamic simulations presented here were performed on cylindrical grids with resolutions of $64 \times 64 \times 64$.

In the binary stability analysis simulations presented in §4, from ~ 2, 600 to 16,700 timesteps were required to follow each binary through one initial orbital period P_I . On the 8K–node MasPar MP–1 at LSU, each timestep took \approx 19 CPU seconds (or \approx 73 µsec per grid zone); hence, these simulations required \approx 14 to 88 CPU hours per P_I . This large range is due to the variation in the size of the integration timestep that could be taken in the different simulations. The size of this timestep is restricted in order to ensure the numerical stability of the computations. The simulations we performed varied in length from 1 P_I to 5 P_I . A few of our binary dynamical stability test simulations were run on the 4K–node MasPar MP–2 at the Scalable Computing Laboratory of the DOE Ames Laboratory at Iowa State University. The CPU time per timestep required for simulations conducted on the MP–2 is about 3/5 that of the time required to run on the MP–1 at LSU.

Our FDH code typically follows the fluid evolution in the inertial reference frame. However, we chose to incorporate the option of running the code in a frame of reference which rotates with the initial angular velocity of the fluid, Ω_0 . This choice was motivated by a desire to minimize numerical effects which might artificially influence the stability of the binary systems studied. The particular effect we sought to minimize was dissipation due to numerical viscosity, which arises from the coarseness of the finite differencing. The hope was that diminishing the motion of the fluid through the grid by running in the rotating reference frame would also diminish the dissipative effects of numerical viscosity on the fluid (see §4 for further details). (We also tried updating the angular velocity of the rotating frame of reference once during some of the simulations presented here, in order to further minimize the dissipation due to numerical viscosity).

The rotating reference frame adds two terms to the radial equation of motion (2) and one to the azimuthal equation (4) (cf., Norman & Wilson 1978):

$$\frac{\partial S}{\partial t} + \nabla \cdot (S\vec{v}) = -\frac{\partial P}{\partial R} - \rho \frac{\partial \Phi}{\partial R} + \frac{A^2}{\rho R^3} + \rho \Omega_0^2 R + \frac{2\Omega_0 A}{R}, \tag{11}$$

$$\frac{\partial A}{\partial t} + \nabla \cdot (A\vec{v}) = -\frac{\partial P}{\partial \phi} - \rho \frac{\partial \Phi}{\partial \phi} - 2\Omega_0 RS.$$
(12)

The $\rho \Omega_0^2 R$ term that has been added to the radial equation of motion results from the centrifugal force; the other two added terms result from the Coriolis force. Note that the centrifugal term in equation (11) can be rewritten as $A'^2/(\rho R^3)$, where $A' \equiv \rho \Omega_0 R^2$. We use this form in the actual computation of the centrifugal term, with A' centered at the same place in each grid cell as is A, in order to be numerically consistent with the computation of the curvature term $A^2/(\rho R^3)$ in the radial equation of motion.

A discussion of the boundary conditions, vacuum treatment, and rotation axis treatment implemented in our hydrodynamics code is presented in New (1996).

3. Equilibrium Sequences

We have constructed hydrostatic equilibrium sequences of synchronized close binaries with polytropic as well as realistic white dwarf and neutron star equations of state. The individual binary models along each sequence have the same equation of state and constant total mass M_T , but decreasing binary separation a. Here a is the distance measured between the pressure [density] maxima of the stellar components. Each such sequence represents a quasistatic approximation to the evolution of a binary system in which gravitational radiation gradually carries away the system's orbital angular momentum. These binary models were constructed, on $128 \times 128 \times 128$ grids, with the HSCF technique (see §2.1), which creates models of rotating, self-gravitating fluid systems in hydrostatic equilibrium.

It should be noted that the true physical viscosity present in double neutron star binaries is not expected to be strong enough to enforce synchronization (Bildsten & Cutler 1992; Kochanek 1992) and the viscosity of the degenerate material in double white dwarf binaries probably is not strong enough to synchronize them either (this can be shown by applying the arguments given in Bildsten & Cutler 1992 to white dwarfs and using the values for the viscosity of degenerate material given in Durisen 1973). However, if magnetic fields are present, they may bring about synchronization. In any case, synchronization is at least a simplifying assumption. Furthermore, since neutron stars have relatively strong gravitational fields, Newtonian models and simulations of double neutron star binaries need to be viewed with caution.

3.1. Polytropic Sequences

The equilibrium sequences that we constructed for binary models with polytropic indices n = 0.5, 1.0, and 1.5 are displayed in Figure 1. For each n, the total energy E and total angular momentum J are plotted versus the separation a. Note that we do not claim that the results given in this figure or in the rest of the manuscript are necessarily accurate to the number of digits in which they are reported; the number of digits in which the results are presented allows the display of characteristics of the equilibrium sequences and the differentiation between individual models on these sequences. As mentioned in §2.1, the equations of state of the polytropic models are such that the total mass of the system M_T does not have to be chosen before its construction, but can be scaled afterwards as desired.

There are in fact three parameters, $M = 1/2M_T$, R_{Sph} , and the polytropic constant K, which set the scale of a polytropic model. Here R_{Sph} is the radius of a spherical star of mass M and polytropic index n. These parameters are related according to the following equation (Chandrasekhar 1967):

$$M = 4\pi m_n \left[\frac{(n+1)K}{4\pi G} \right]^{\frac{-(3+n)}{2(1-n)}} \left[\frac{R_{Sph}}{r_n} \right]^{\frac{(3-n)}{(1-n)}},$$
(13)

where m_n and r_n are Lane-Emden constants for a particular value of n (see Table 1 for their values

corresponding to n = 0.5, 1.0, and 1.5). Thus, only two of these three parameters are independent; if two of them are specified, the other one is automatically determined. The quantities in Figure 1 are themselves normalized to G, M, and R_{Sph} . Specifically, E has been divided by $(GM^2R_{Sph}^{-1})$; Jhas been divided by $(G^{1/2}M^{3/2}R_{Sph}^{1/2})$; and a has been divided by R_{Sph} .

In the discussion that follows, as in Figure 1, all values of the binary separation a have been normalized to R_{Sph} . On each sequence, Point C marks the system where the surfaces of the two binary components just come into contact. Systems to the right of this point are detached binaries and systems to left are contact binaries or "dumbbells." For the sake of illustration, Figure 2 displays an isodensity surface image of an example detached binary model (a = 3.28, n = 1.0) and of an example dumbbell model (a = 2.70, n = 1.0). Points M mark the models along each sequence which have the minimum total energy and the minimum total angular momentum. Along all three polytropic sequences, the minimum in E occurs at the same separation as the minimum in J. (See §3.4 below for a discussion of the significance of these minima.) The model with the smallest separation on each sequence, marked with a T, will be referred to as the "terminal" model. No synchronously rotating binary models with the equation of state particular to that sequence can be constructed in equilibrium with a smaller separation than that of the terminal model because the centrifugal force would exceed the gravitational force along the equator of such systems.

The separation at which this termination of the sequence occurs increases from a = 2.45 for n = 1.5 to a = 2.76 for n = 0.5. The separation at which the minima occur also increases from a = 2.70 for n = 1.5, to a = 2.89 for n = 1.0, to a = 3.11 for n = 0.5. Note that contact occurs to the right of the minima for n = 1.5 and to the left of the minima for n = 1.0 and 0.5. We have determined that Points C and M coincide for n = 1.177. If the binary components were spherical, their separation at the point of contact would be a = 2. However, a(C) ranges from 2.81 for n = 1.5 to 2.94 for n = 0.5.

3.1.1. Comparison with Previous Work

In this section, we compare our polytropic equilibrium sequences to those of LRS (1993b) and RS (1992, 1995). Note that LRS (1993b) and RS (1992, 1994, 1995) define binary separation as the distance between the centers of mass of the binary components and, as mentioned above, we define it as the distance between the pressure (density) maxima of the components. For ease of comparison, the values of binary separation presented in this section that are based on our work do represent the separation between the centers of mass of our binary components. In this section and the rest of this manuscript, any binary separation which refers to the distance between the components centers of mass will be denoted as a_{cm} .

The analytical stability analyses of LRS (1993b), which utilized an approximate energy variational technique, also showed that simultaneous minima in E and J existed along sequences of constant mass, synchronized binaries with n = 0.5, 1.0 and 1.5. (According to LRS 1993b, the

minima occur at $a_{cm} = 2.99$ on the n = 0.5 sequence and at $a_{cm} = 2.76$ on the n = 1.0 sequence.) This analytical method cannot construct contact binaries and thus, according to our sequences, should not be able to identify minima on the n = 1.5 sequence. However, because the n at which the minima and points of contact coincide is ~ 2.0 in their study, LRS (1993b) do find minima for the n = 1.5 sequence at $a_{cm} = 2.55$.

In addition, approximate equilibrium sequences were constructed with the SPH techniques of RS (1992, 1995). The n = 1.0 sequence presented in LRS (1993b) has simultaneous minima at $a_{cm} = 2.90$, which is closer to our value of $a_{cm} = 2.98$ than the analytically determined $a_{cm} = 2.76$ of LRS (1993b). The n = 1.5 sequence presented in RS (1995) has the minima at $a_{cm} = 2.67$. No sequence with n = 0.5 has been published by RS. Table 2 contains a summary of the separations a_{cm} of the models at the minima of the polytropic sequences as determined in LRS (1993b), RS (1995), and this work. For completeness, this table also gives the values of binary separation determined by this work in terms of the separation a between the pressure maxima of the components.

Hachisu (1986b) also shows equilibrium sequences of n = 0.5 and 1.5 polytropes. However he presents his results as sequences of Ω_0^2 versus J^2 instead of E or J versus a. A comparison between Hachisu's (1986b) results and ours is given in Figure 3. To conform with Hachisu's notation, the quantities in this figure are normalized to $4\pi G$, M_T , and V_T , where V_T is the total volume of the binary system. Specifically, Ω_0^2 has been divided by $(4\pi G M_T/V_T)$ and J^2 has been divided by $(4\pi G M_T^3 V_T^{1/3})$.

3.2. White Dwarf Sequences

We have constructed equilibrium sequences for binary models with the zero-temperature WD equation of state. Because the HSCF technique requires that the maximum density of the desired model (which sets M_T) be given as input when this equation of state is used, it is impossible to build a single sequence that can be scaled to any desired M_T with this equation of state. Instead we have constructed separate WD sequences, each of which represents models with one specific value of M_T . We have constructed nine such sequences with M_T ranging from .298 M_{\odot} to 2.72 M_{\odot} . Four representative sequences, with $M_T = .500, 1.19, 2.03, \text{ and } 2.72 M_{\odot}$, are shown in Figure 4. The other five sequences are displayed in Appendix A, along with the four WD sequences presented in Figure 4. (In addition, two WD sequences with M_T [near $2M_{CH}$] = 2.81 and 2.85 are presented in Appendix A; they have been excluded from the discussion below because of their irregular nature.) The normalization in Figure 4 is the same as that in Figure 1. However, in this case R_{Sph} has been determined numerically by constructing a spherical white dwarf of mass $M = M_T/2$ in hydrostatic equilibrium.

The separations a of the models at the points of contact, the minima, and the terminal points on the constructed white dwarf equilibrium sequences are shown in Figure 5 as a function

of the total binary system mass. Along the WD sequences, the separation of the terminal model gradually increases from a = 2.45 when $M_T = .298 M_{\odot}$ to a = 2.86 when $M_T = 2.72 M_{\odot}$. As in the polytropic sequences presented in the previous section, simultaneous minima in E and J exist along each WD sequence. The point of contact on these sequences always occurs at a larger separation than the minima; the separation at which it occurs also gradually increases from a = 2.81 for $M_T = .298 M_{\odot}$ to a = 3.05 for $M_T = 2.72 M_{\odot}$ (except for a slight decrease in this separation for the $M_T = 1.19 M_{\odot}$ sequence). The separation of the model at the minimum of each sequence also increases from a = 2.70 for $M_T = .298 M_{\odot}$ to $a = 2.72 M_{\odot}$; however, in this case there is a somewhat more substantial decrease in this separation between the $M_T = .500 M_{\odot}$ and $M_T = 2.36 M_{\odot}$ sequences (for which a = 2.73).

3.2.1. Comparison with Previous Work

Hachisu (1986b) has constructed double white dwarf binary sequences along which ρ_{max} , instead of M_T , was held constant. Figure 6 shows a comparison between the J versus M_T relations for the models with the minimum angular momentum on the Hachisu (1986b) sequences and those on our sequences. The angular momentum in this figure is normalized to 10^{50} in cgs units and the mass is normalized to M_{\odot} . The comparison is excellent for low masses, however the relations deviate slightly for $M_T \geq 2 M_{\odot}$.

3.3. Neutron Star Sequences

We have constructed equilibrium sequences for binary models with three realistic NS equations of state of varying compressibility (F, soft; FPS, medium; L, hard). As in the case of the WD equation of state, the desired M_T for each of these sequences must be specified prior to their construction. We have chosen to construct one sequence with $M_T = 2.80 M_{\odot}$ for each of the three equations of state. These three sequences are displayed in Figure 7 and have been normalized to G, M, and R_{Sph} . The values of R_{Sph} were determined numerically by constructing a spherical star of mass $M = M_T/2$, in hydrostatic equilibrium, with each of the three NS equations of state.

The terminal model occurs at the same separation on the F and FPS sequences (a = 2.59)and at a slightly wider separation (a = 2.62) on the L sequence. The locations of the minima in E are not very well defined on these sequences. For the F sequence, the E minimum likely occurs in the range 2.75 < a < 2.81; for the FPS sequence, in the range 2.72 < a < 2.81; and for the L sequence, in the range 2.72 < a < 2.84. The J minima are well defined and occur at nearly the same separation on all three sequences (on the F sequence at a = 2.80, on the FPS sequence at a = 2.78, and on the L sequence at a = 2.79). Like the white dwarf sequences, the minima always occur at a smaller separation than the points of contact. However, on all of the neutron star sequences these two points are very close together. The separation between points C and M thus seems to be determined by the lower density regions of the objects since this is where the equations of state, which differ significantly only in the density regimes above nuclear density $(2.8 \times 10^{14} \text{ g cm}^{-3})$, are similar.

The scatter in E displayed near the minima of these sequences may result in part from our piecemeal reconstruction of Cook's (1995) tabular NS equations of state (see §2) and from the approximate manner in which we calculate the internal energy E_{int} of the models (we compute an effective polytropic index n_{eff} for each grid zone in the model and then use these spatially varying indices to calculate the internal energy according to $E_{int} = \int n_{eff} P \, dV$). Because of these factors, we identify the J minima as the true minima along these sequences and, as before, have marked their location with the letter M. Another factor which must be kept in mind when studying the features of these NS sequences is that the virial error (VE), which measures the quality of the equilibria, is $\sim 10^{-2}$. This is one to two orders of magnitude higher than the VE of models along the polytropic and WD equation of state sequences and almost certainly results in part from the piecemeal forms of the NS equations of state used. Note that for the polytropic and WD equation of state, we typically very accurately pinpointed the location of the minimum by moving point B (one of the two points on the surface of the star that must be given as input to the HSCF code and whose position influences the separation of the binary components) one grid cell at a time in the region of the minimum in order to get as many models as possible with the grid resolution we used. However, since we had difficulty obtaining converged models for some portions of the NS sequences, we moved point B two grid cells at a time when constructing NS models. Thus the locations of the minima are slightly more uncertain for the NS equations of state than in the other studied equations of state.

3.4. Nature of the Minima

Turning points on equilibrium sequences, like the minima present in E and J along the sequences presented above, are usually associated with points of instability. The two types of instability which will be discussed below are *secular* instability and *dynamical* instability. For an instability to be classified as dynamical, according to the convention of LRS (1993b), it must conserve energy, angular momentum, and circulation. If an instability proceeds as a result of some mechanism that dissipates one of the conserved quantities, e.g., via viscosity or gravitational radiation, then it is classified as a secular instability (see also Tassoul [1978] for discussions of dynamical versus secular instabilities). A dynamical instability takes place on the dynamical timescale of the system; a secular instability takes place on the timescale of the particular dissipative mechanism which induces it.

The minima in E and J on synchronous binary sequences have been identified as points of secular instability by previous authors. LRS (1993b) stated that the neighboring models adjacent to the model at the minimum of each sequence are uniformly rotating and therefore can only be reached with the aid of viscosity. Thus they concluded that this minimum cannot be associated with a dynamical instability since viscosity does not preserve circulation. Their approximate analytical method predicts that on polytropic sequences with n < 0.7, dynamical instabilities exist at separations smaller than those of the minima. For the n = 0.5 sequence, these authors conclude that the dynamical instability sets in at $a_{cm} = 2.68$. Hachisu (1986b and references therein) also labels turning points along his synchronous polytropic and WD sequences as points of secular instability.

Because our hydrodynamics code does not include the dissipative effects of either the gravitational radiation reaction or the true fluid viscosity, we are unable to confirm the presence of a secular instability with a hydrodynamics simulation. However, it is possible to study the dynamical stability of a system with our code. In the following section, we present the results of our FDH tests of the dynamical stability of models on sequences selected from those presented above and compare these results with those of other authors.

4. Hydrodynamic Tests of Stability

To determine if a point of dynamical instability exists on an equilibrium sequence like those discussed in the previous section, the dynamical stability of individual models along the sequences may be tested with FDH simulations. We have done just that for the three polytropic sequences of §3.1; for a low mass ($M_T = .500 M_{\odot}$) and a high mass ($M_T = 2.03 M_{\odot}$) WD sequence from §3.2; and for two of the three realistic NS equations of state sequences of §3.3.

All of these stability tests were performed in the rotating reference frame (§2.2) in order to minimize the dissipative effects of the numerical viscosity which results from the discrete nature of the computational simulation. The influence of numerical viscosity on the evolution of binary systems can be seen in Figure 8 which shows a comparison between simulations of one particular WD binary system ($M_T = .500 M_{\odot}$ and a = 2.63) performed in the inertial frame (dashed curve) and in the rotating frame (solid curve). This figure shows the evolution of the moment of inertia of the system I, as a function of time t. The evolution of I is more instructive than the evolution of the binary separation itself since the latter quantity can only be measured by discrete jumps in the location of the density maximum on the grid, whereas I varies smoothly with time.

As can be seen from Figure 8, the binary appears to be dynamically unstable when the simulation is performed in the inertial frame (dashed curve), as I plummets on a timescale of 2–3 P_I . By contrast, the same model evolved in the rotating frame is certainly not unstable to merger, as can be seen by the relatively steady behavior of its moment of inertia over time. Thus, simulations done in the rotating frame prevent the misidentification of models as dynamically unstable, which are so only because of numerical artifacts. In order to illustrate that the accuracy of the finite differencing scheme also influences the amount of numerical viscosity present in a simulation, Figure 8 also shows the same model evolved in the rotating frame but with a FDH code that used a first–order accurate advection scheme to compute the divergence terms in equations

(1-4) (dot-dashed curve). This figure indicates that the accuracy of the code has an effect on the evolution of this system that is similar to that of the flow of the fluid through the grid in the inertial frame.

Models along the equilibrium sequences presented in §3 were constructed with a grid resolution of $128 \times 128 \times 128$. However, a FDH simulation with this resolution cannot be done on the MP–1 computer at LSU. So portions of the selected sequences mentioned above have been recomputed on $64 \times 64 \times 64$ grids. It is the stability of models on these new sequences which actually has been tested. For completeness, Table 3 gives the separations of the points of contact, minima, and terminal models for both the 64^3 and the 128^3 versions of the polytropic and WD sequences discussed below. (We do not show this comparison for the NS sequences because we have not determined or were unable to accurately determine the location of some of these points on the 64^3 NS sequences.)

4.1. White Dwarf Sequences

4.1.1.
$$M_T = 2.03 M_{\odot}$$

In the lower panel of Figure 9, I(t) is shown for WD binaries $(M_T = 2.03 M_{\odot})$ with separations ranging from a = 2.80 (triple dot-dashed curve, a dumbbell model just past the point of contact) to a = 2.53 (solid curve; the terminal model on the sequence). For the sake of convenience, the relevant equilibrium sequence itself is reprinted in the upper panel of Figure 9. The moments of inertia of the binary models at the points of contact, minima, and termination along the equilibrium sequence (constructed on a $128 \times 128 \times 128$ grid) are labelled with the letters M, C, and T, respectively. Note that because the binary models used in the FDH stability tests were from sequences constructed on $64 \times 64 \times 64$ grids, there may be a slight offset between the initial values of I for these models and the points marked as M, C, and T on the I(t) plot since they correspond to the $128 \times 128 \times 128$ sequence.

All of the models tested on the sequence are dynamically stable. Thus we conclude that no point of dynamical instability exists along this sequence. In Figure 10, we present isodensity images of an example of the evolution of a stable binary. The images are from the simulation of the model at the minimum of the $M_T = 2.03 M_{\odot}$ sequence, corresponding to the dot-dashed curve of Figure 9. Since the simulation was performed in the rotating frame, the binary does not appear to pivot very much in this set of images even though the simulation was carried out for ~ $4P_I$.

4.1.2.
$$M_T = .500 M_{\odot}$$

Our tests of the $M_T = 2.03 M_{\odot}$ sequence began with models of wider separation and continued up the sequence to the terminal model. Because no point of dynamical instability was found on this sequence, we performed our tests of the $M_T = .500 M_{\odot}$ sequence on models much closer to the terminal model, knowing that we could work our way back down the sequence to the point of dynamical instability if we found models which were unstable. (This methodology assumes that all models which have separations less than that of the model located at the point of dynamical instability will also be unstable.) But, as can be seen from the bottom panel of Figure 11, both a model at a = 2.63 (dashed curve) and the terminal model at a = 2.45 (solid curve) are dynamically stable against merger. Thus we again infer that there is no point of dynamical instability along this sequence.

4.2. Polytropic Sequences

4.2.1.
$$n = 1.5$$

Based on the results of the stability tests of the WD sequences, we began our investigation of this sequence with the terminal model (a = 2.45). Because an n = 1.5 polytrope is supposed to be a fair representation of a low mass WD, we have plotted the I(t) of the terminal model (a = 2.45) in Figure 11 (dot-dashed curve) along with the models of the low mass WD sequence. The polytropic model has been scaled to represent a binary with $M_T = .500 M_{\odot}$ and a R_{Sph} equal to that of a spherical WD with the same mass. This sets K according to equation 13. As can be seen, the evolution of the n = 1.5 terminal model closely follows that of the low mass WD terminal model. From its stability, we infer that the remainder of the models on the n = 1.5 sequence are also stable and thus no point of dynamical instability exists along this sequence either. This result conflicts with the SPH simulations of RS (1995) which identified a point of dynamical instability at $a_{cm} \simeq 2.4$ on their n = 1.5 sequence.

4.2.2. n = 1.0

As Figure 12 illustrates, we have performed dynamical stability tests of four binaries on the n = 1.0 sequence with separations ranging from a = 3.28 (triple dot-dashed curve) to a = 2.62 (solid curve; terminal model). All were stable against merger on a dynamical timescale. The moment of inertia of the terminal model actually increases by about 20% over the timescale $t = 4P_I$ depicted here; the moment of inertia of the initially most widely separated model (a = 3.28) decreases by about the same percentage. The two other models exhibit behavior in between these two extremes. Note that after an initial dip, the moment of inertia of the model at the minimum of the sequence (a = 2.88, the dot-dashed curve) is nearly constant. These results conflict with the SPH simulations of RS (1992) which identified a model with $a_{cm} = 2.8$ as being dynamically unstable.

4.2.3.
$$n = 0.5$$

As Figure 13 illustrates, we have tested the dynamical stability of five binaries on the n = 0.5 sequence with separations ranging from a = 3.41 (long dashed curve) to a = 2.77 (solid curve; terminal model). Both the model at the minimum of the sequence (a = 3.10-short dashed curve) and the terminal model were unstable to merger on a dynamical timescale. The other three more widely separated models, including the model (a = 3.17-dot-dashed curve) located just prior to the minimum of the sequence, were stable. Thus dynamical instability sets in at the minimum of this sequence (a = 3.10, $a_{cm} = 3.20$). The SPH simulations of RS (1994) identified a point of dynamical instability along this sequence at $a_{cm} = 2.97$.

4.3. Neutron Star Sequences

4.3.1. Equation of State L

As Figure 14 illustrates, we have tested the dynamical stability of a NS binary system near the minimum (a = 2.79) and a more widely separated model (a = 3.26) on the realistic neutron star equation of state L sequence. The model near the minimum of the sequence became unstable to dynamical merger in one P_I . The more widely separated model appears to be stable; its behavior resembles that of the most widely separated models tested on the n = 1.0 and 0.5 sequences (see Figures 12 and 13). Although we have not accurately identified the separation at which the dynamical instability sets in along this sequence, it has obviously already done so at a = 2.79. By analogy with the n = 0.5 sequence, it is possible to infer that the onset of dynamical instability is associated with the region of the minimum energy and angular momentum along the sequence.

4.3.2. Equation of State F

As Figure 15 illustrates, we have tested the dynamical stability of the model at the minimum (a = 2.80) of the realistic neutron star equation of state F sequence. Like the model near the minimum of the equation of state L sequence, the model at the minimum of this sequence is also unstable to dynamical merger. Although we have not tested the stability of a widely separated model on this sequence, we infer, by analogy with the n = 0.5 and equation of state L sequences, that there exist more widely separated models on this sequence that are stable and that the point of onset of the dynamical instability may be associated with the region of the minimum.

4.3.3. Equation of State FPS

We have not tested the stability of any of the models on the realistic NS equation of state FPS sequence. However, since our tests of the stiff equation of state L and the soft equation of state F produced similar results, we expect that the stability properties of the models on this equation of state of medium stiffness will resemble the properties of models on these other realistic NS equations of state sequences.

5. Discussion and Conclusions

We have examined the dynamical stability of synchronously rotating, equal-mass binaries with polytropic, zero-temperature white dwarf, and realistic neutron star equations of state. Specifically, we tested the dynamical stability of individual models constructed along equilibrium sequences of binaries with the same total mass M_T and equation of state but decreasing separation, in order to determine if any models on these sequences were unstable to merger on a dynamical timescale.

Our stability analyses started with two white dwarf (WD) equation of state sequences, one with a low total mass ($M_T = .500 M_{\odot}$) and one with a fairly high total mass ($M_T = 2.03 M_{\odot}$), used as representatives of the nine regular WD equation of state sequences we constructed (which ranged in mass from $M_T = .298$ to $2.72 M_{\odot}$). Our simulations indicate that no points of dynamical instability exist on either of these two sequences. We have inferred from this result, that it is likely (although not certain) that the other WD sequences are also dynamically stable. This being the case, we expect that WD mergers will only happen via secular processes and that it will not be possible to properly simulate the coalescence of equal-mass double white dwarf binaries using explicit FDH (or SPH) techniques. It still remains to be seen whether or not double white dwarf binaries having unequal mass components are susceptible to merger on a dynamical timescale.

Our examination of the n = 1.5 and n = 1.0 polytropic sequences also identified no points of dynamical instability. This result conflicts with the published results of RS (1992, 1995) who identified a dynamically unstable binary between the minimum and the terminal point of the n = 1.5 sequence and another just past the minimum of the n = 1.0 sequence. However, like RS (1994), our test of the n = 0.5 sequence does indicate the presence of a dynamical instability. In our simulations, this instability sets in at the minimum of the sequence. RS (1994) locate the point of dynamical instability at $a_{cm} = 2.97$. Although they do not state where the minimum of their sequence is located, the analytical work of LRS (1993b) places it at $a_{cm} = 2.99$. Recall that LRS (1993b) label this minimum as a secular instability and they predict that a dynamical instability sets in at a smaller separation ($a_{cm} = 2.68$) on this sequence. However, in light of the simulations of RS (1994) and of this work, it seems likely that the minimum itself may be associated with the onset of the dynamical instability. The differences between our results and those of RS (1992, 1995) for the sequences with the softer equations of state may result from the fact that SPH has difficulty modeling low density regions that are more extensive in systems with softer equations of state. It is interesting to note that the analytical work of LRS (1993b) predicts that points of dynamical instability exist only on sequences for which n is less than ≈ 0.7 . It would be intriguing to test the stability of other polytropic sequences with our FDH code in order to determine at what value of n the dynamical instability first appears. Another point that is worth emphasizing again, is that our stability tests were run in the rotating frame of reference. We believe that we would have misidentified some truly stable models as being unstable had these tests been performed in the inertial frame (see the discussion in §4 associated with Figure 8).

Our stability analyses of the realistic neutron star (NS) equations of state sequences identified models at (or near) the minima of the soft equation of state F and the hard equation of state L as being dynamically unstable. However, because of computing resource constraints we have been unable to determine whether or not the *onset* of the dynamical instability takes place in the regions of the minima of these sequences. If the n = 0.5 sequence is taken as an example, one might infer this to be the case. Although we did not test the stability of the medium equation of state FPS sequence we constructed, we expect that such tests would yield results similiar to those of the other two NS equations of state. If further simulations of the n = 0.5 and NS equations of state sequences do identify the minimum as the point of dynamical instability, the question will arise as to why this turning point does not also mark the onset of dynamical instability on the sequences with softer equations of state. At this time we are unable to provide a physical explanation for this possibility (see, however, the discussion in LRS [1993b]).

All of the binary models that we have identified as stable against dynamical merger in §4 have not necessarily become steady-state configurations by the end of our simulations. In fact, at the end of our simulations the moments of inertia of some of the stable models are still decreasing gradually and those of others are still increasing gradually. However, these binaries did not become unstable to merger on a dynamical timescale (i.e., \sim a few P_I).

It is interesting to note that this gradual (secular-type) evolution of our models is such that models before the minimum of a sequence (i.e., models with separations larger than that of the model at the minimum) tended to exhibit decreasing moments of inertia and those after the minimum tended to exhibit increasing moments of inertia. (This trend appears in the simulations of models on the low mass white dwarf sequence and is more pronounced in the tests of models with stiffer equations of state.) LRS (1994b) have indicated that viscosity does indeed cause the orbits of models before the minimum of a sequence to decay. They also suggest that as a result of the action of viscosity, the orbit of a binary past the minimum "... can either expand ... as the system is driven to a lower energy, stable synchronized state, or it can decay ... as the stars are driven to coalescence."

The LRS (1994b) description of the action of viscosity is consistent with our results if the

gradual evolution of the moments of inertia of our models is attributed to the effects of the remaining numerical viscosity in our code (which acted in our case to *increase* the moments of inertia of dynamically stable models past the minima). By carrying out simulations in the rotating reference frame (as is illustrated in Figure 8), we have overcome the primary effect of numerical viscosity, which is to dissipate orbital motions and drive systems to coalescence. In simulations performed in the rotating frame, it may be a higher order effect of numerical viscosity on any internal motions that develop in the systems that causes the observed secular–type evolution of our binary models. Note that this higher order effect of numerical viscosity cannot be identified as the mechanism responsible for driving any of our unstable models to coalescence because the timescale of their evolution was dynamical and not gradual. In addition, had this aspect of numerical viscosity played a significant role in the evolution of the terminal model on the n = 0.5 sequence, its moment of inertia should have increased gradually, but instead its moment of inertia decreased and the model merged on a dynamical timescale.

Even though our work indicates that there is no point of dynamical instability along the n = 1.0 sequences, it would still be possible for an explicit hydrodynamics code to follow the merger of a close binary with this equation of state if it was assumed to represent a neutron star–neutron star system. This is because the timescale, τ , on which gravitational radiation would drive a close neutron star–neutron star binary to coalescence is on the order of its initial orbital period, P_I . According to Shapiro & Teukolsky (1983), a point mass approximation to this timescale is

$$\tau = \frac{5}{256} \frac{c^5}{G^3} \frac{a^4}{2M^3}.$$
(14)

If the binary at the minimum of our n = 1.0 sequence is assumed to have components with $M = 1.4 M_{\odot}$ and $R_{Sph} = 10$ km, then $\tau = 2.5$ ms $= 1.6 P_I$. (Note that for the binary at the minimum of our $M_T = 2.03 M_{\odot}$ WD equation of state sequence, $\tau P_I^{-1} = 2.2 \times 10^7$ and for the binary with a = 2.63 on our $M_T = .500 M_{\odot}$ WD equation of state sequence, $\tau P_I^{-1} = 6.4 \times 10^9$.) Hence, if the effects of the gravitational radiation reaction were accounted for, as other authors have done (e.g., Oohara & Nakamura 1990; Davies et al. 1994; Zhuge, Centrella, & McMillan 1994; Ruffert, Janka, & Schäfer 1996), the merger of the n = 1.0 binary would proceed on a timescale comparable to the dynamical timescale.

The variation between the results of our stability analyses of binaries with the softer equations of state and those of RS (1992, 1995) emphasizes the importance of comparing the results of hydrodynamic simulations performed with different numerical techniques. Certainly the inclusion of more complex physics, such as the effects of the gravitational radiation reaction and of full general relativity should be the aim of research in this field. However, an effort should be made to reach agreement on the results of much simpler, Newtonian simulations in order that their results and the results of more complex simulations can be confidently presented as guides to those who will be designing and building gravitational radiation detectors and interpreting the data collected at future gravitational radiation observatories. This work has been supported, in part, by funding from the National Science Foundation through grants AST-9008166, AST-9528424, and PHY-9208914, from NASA through grants NAGW-2447 and NAG5-2777, from the Louisiana State Board of Regents through grant LEQSF (1995-1998)-115-35-4412, and from the Baton Rouge, Louisiana Branch of the American Association of University Women through a Doctoral Candidate Scholarship and by computational resources from the Pittsburgh Supercomputing Center through grant PHY910018P. The great majority of the numerical simulations presented herein were carried out on computers in the Department of Physics and Astronomy's Concurrent Computing Laboratory for Materials Simulation which was established through grants LEQSF(1990-92)-ENH-12 and LEQSF(1993-94)-ENH-TR05 from the Louisiana State Board of Regents. Several of the numerical simulations also were carried out at the Scalable Computing Laboratory of the DOE Ames Laboratory at Iowa State University. We would also like to thank Joan Centrella, Dimitris Christodoulou, Greg Cook, Dong Lai, Dustin Laurence, Kip Thorne, and Horst Väth for useful conversations and assistance.

A. Equilibrium Sequences

Eleven WD equation of state equilibrium binary sequences, each with a different M_T , are displayed in Figure 16. See §3.2 for details.

REFERENCES

- Abramovici, et al. 1992, Science, 256, 325
- Bildsten, L., & Cutler, C. 1992, ApJ, 400, 175
- Branch, D., Livio, M., Yungelson, L. R., Boffi, F. R., & Baron, E. 1995, PASP, 107, 1019
- Chandrasekhar, S. 1967, An Introduction to the Study of Stellar Structure (New York: Dover)
- Chen, K., & Leonard, P. J. T, 1993, ApJ, 411, L75
- Cohl, H. S., Sun, X.-H., & Tohline, J. E. 1997, in Proceedings of the 8th SIAM Conference on Parallel Processing for Scientific Computing, in press
- Colgate, S. A., & Petschek, A. G. 1982, Nature, 296, 804
- Cook, G. B. 1995, private communication
- Cook, G. B., Shapiro, S. L., & Teukolsky, S. A. 1994, ApJ, 424, 823 (CST)
- Cutler, C., et al. 1993, Phys. Rev. Lett., 70, 2984
- Davies, M. B., Benz, W., Piran, T., & Thielemann, F. K. 1994, ApJ, 431, 742
- Eichler, D., Livio, M., Piran, T., & Schramm, D. N. 1989, Nature, 340, L126
- Faller, J. E., Bender, P. L., Hall, J. L., Hils, D., Stebbins, R. T., & Vincent, M. A. 1989, Adv. Space Res., 9, 107
- Friedman, J. L., Ipser, J. R., & Parker, L. 1986, ApJ, 304, 115
- Gingold, R. A., & Monaghan, J. J. 1979, MNRAS, 188, 45
- Hachisu, I. 1986a, ApJS, 61, 479
- Hachisu, I. 1986b, ApJS, 62, 461
- Hachisu, I., & Eriguchi, Y. 1984a, PASJ, 36, 239
- Hachisu, I., & Eriguchi, Y. 1984b, PASJ, 36, 259
- Hough, J., et al. 1995, in Proceedings of the First Edoardo Almadi Conference on Gravitational Wave Experiments, ed. E. Coccia, G. Pizzella, & F. Ronga (Singapore: World Scientific), 50
- Iben, I., Jr. 1988, ApJ, 324, 355
- Iben, I., Jr. 1990, ApJ, 353, 215
- Iben, I., Jr. 1991, ApJS, 76, 55
- Iben, I., Jr., & Tutukov, A. V. 1984, ApJS, 54, 335
- Iben, I., Jr., & Tutukov, A. V. 1986, ApJ, 311, 753
- Iben, I., Jr., & Webbink, R. 1989, in White Dwarfs, ed. G. Wegner (Berlin: Springer), 377
- Janka, H.-Th., & Ruffert, M. 1996, A&A, 307, L33

- Katz, J. I., & Canel, L. M. 1996, ApJ, 471, 915
- Kawai, Y., Saio, H., & Nomoto, K. 1987, ApJ, 315, 229
- Kochanek, C. S. 1992, ApJ, 398, 234
- Lai, D., Rasio, F. A., & Shapiro, S. L. 1993a, ApJ, 406, 63
- Lai, D., Rasio, F. A., & Shapiro, S. L. 1993b, ApJS, 88, 205
- Lai, D., Rasio, F. A., & Shapiro, S. L. 1994a, ApJ, 420, 811
- Lai, D., Rasio, F. A., & Shapiro, S. L. 1994b, ApJ, 423, 344
- Lipunov, V. M., Postnov, K. A., Prokhorov, M. E., & Panchenko, I. E. 1995, ApJ, 454, 593
- Meers, B. J. 1988, Phys. Rev. D, 38, 2317
- Merkowitz, S. M., & Johnson, W. W. 1995, Phys. Rev. D, 51, 2546
- Meyer, B. S. 1989, ApJ, 343, 254
- Narayan, R., Paczński, B., & Piran, T. 1992, ApJ, 395, L83
- New, K. C. B. 1996, Ph.D. thesis, Louisiana State University, Baton Rouge
- Norman, M. L., & Wilson, J. R. 1978, ApJ, 224, 497
- Oohara, K., & Nakamura, T. 1990, Prog. Theo. Phys., 83, 906
- Rasio, F. A., & Shapiro, S. L. 1992, ApJ, 401, 226 (RS 1992)
- Rasio, F. A., & Shapiro, S. L. 1994, ApJ, 432, 242 (RS 1994)
- Rasio, F. A., & Shapiro, S. L. 1995, ApJ, 438, 887 (RS 1995)
- Ruffert, M., Janka, H.-Th., Schäfer, G. 1996, A&A, 311, 532
- Saio, H., & Nomoto, K. 1985, A&A, 150, L21
- Shapiro, S. L., & Teukolsky, S. A. 1983, Black Holes, White Dwarfs, and Neutron Stars (New York: Wiley)
- Shibata, M., Nakamura, T., & Oohara, K. 1993, Prog. Theo. Phys., 89, 809
- Strain, K. A., & Meers, B. J. 1991, Phys. Rev. Lett., 66, 1391
- Tassoul, J-L. 1978, Theory of Rotating Stars, (Princeton: Princeton University Press)
- Thorne, K. S. 1995, in Proceedings of the Snowmass 95 Summer Study on Particle & Nuclear Astrophysics, & Cosmology, ed. E. W. Kolb, & R. Peccei (Singapore: World Scientific), p. 398
- Tohline, J. E. 1978, Ph. D. Thesis, University of California, Santa Cruz
- Webbink, R. F. 1984, ApJ, 277, 355
- Wilson, J. R., & Mathews, G. J. 1995, Phys. Rev. Lett., 75, 4161
- Woodward, J. W. 1992, Ph. D. thesis, Louisiana State University, Baton Rouge

Woodward, J. W., Tohline, J. E., & Hachisu, I. 1994, ApJ, 420, 247

Zhuge, X., Centrella, J. M., & McMillan, S. L. W. 1994, Phys. Rev. D, 50, 6247

This preprint was prepared with the AAS ${\rm IAT}_{\rm E}{\rm X}$ macros v4.0.

FIGURE CAPTIONS

Fig. 1.–Polytropic Equilibrium Sequences. Sequences of binaries with polytropic indices n = 0.5, 1.0, and 1.5 are displayed. Each sequence displays the total energy E and the total angular momentum J of synchronized equilibrium binaries with the same total mass M_T but changing separation a. See the text (§3.1) for details on how to scale the M_T of each polytropic sequence. Quantities have been normalized to G, $M = M_T/2$, and R_{Sph} , where R_{Sph} is the radius of a spherical polytrope of mass M and polytropic index n. Points M mark binary systems with the minimum E and J along each sequence. Points C mark the system where the surfaces of the stars come into contact. Points T mark the terminal model.

Fig. 2.–Images of a Detached Binary and a Dumbbell. Example isodensity images of a detached binary and a contact binary, or "dumbbell." These two binaries have n = 1.0; the separation of the detached binary shown in Figure 2a is a = 3.28; the separation of the dumbell shown in Figure 2b is a = 2.70. The density level is 5.0×10^{-3} of the maximum density.

Fig. 3.–Comparison with Hachisu's Polytropic Sequences. The square of the angular velocity Ω_0 versus the square of the total angular momentum J of equilibrium binaries with the same total mass M_T but decreasing separation a is shown for both the n = 0.5 and 1.5 sequences of Hachisu (1986b, individual models connected by solid lines) and for our sequences (individual models marked with +'s). The quantities are normalized to $4\pi G$, M_T , and V_T , the total volume of the system.

Fig. 4.–White Dwarf Equilibrium Sequences. The same as Figure 1 but for binaries with the zero–temperature white dwarf equation of state. Because, unlike the polytropes, the M_T of these systems cannot be scaled, separate sequences must be constructed for binaries with different M_T . Four representative sequences with $M_T = .500$, 1.19, 2.03, and 2.72 M_{\odot} are shown here. In Appendix A, sequences for seven other values of M_T are shown, along with those given here. The normalization is the same as in Figure 1, but here R_{Sph} is the radius of a spherical model with the WD equation of state and mass $M = M_T/2$.

Fig. 5.–Separation of Models on White Dwarf Equilibrium Sequences. The separation a of the models at the points of contact (×), the minima (asterisks), and the terminal points (plusses) on the white dwarf equilibrium sequences are shown as a function of the total mass M_T of the binaries on those sequences.

Fig. 6.–Comparison with Hachisu's White Dwarf Sequences. The total angular momentum J versus the total mass M_T of the models with the minimum J on each of Hachisu's (1986b) constant maximum density sequences (individual models marked with \times 's) and on each of our constant M_T sequences (individual models marked with +'s). The angular momentum has been normalized to 10^{50} in cgs units and the total mass to M_{\odot} .

Fig. 7.–Neutron Star Equilibrium Sequences. The same as Figure 1 but for binaries with the F, FPS, and L realistic neutron star equations of state. The M_T on each of these sequences is 2.80

 M_{\odot} (unlike polytropes, the M_T of these systems cannot be scaled). The normalization is the same as in Figure 1 but here R_{Sph} is the radius of a spherical model constructed with the particular NS equation of state of the sequence and a mass $M = M_T/2$.

Fig. 8.–Comparison of Stability Tests Performed with Different Numerical Techniques. The moment of inertia I, normalized to (MR_{Sph}^2) , as a function of time t, normalized to the initial orbital period P_I , is given for dynamical stability tests of a binary with the zero–temperature white dwarf equation of state, $M_T = 0.500 M_{\odot}$, and a = 2.63. The solid curve shows the results of a simulation performed with our second–order accurate FDH code in the rotating frame; the dashed curve shows the test performed with the same code but in the inertial frame; and the dot–dashed curve shows the test performed in the rotating frame, but with the advection terms in the FDH code reduced to first–order accuracy.

Fig. 9.–Stability Tests of the $M_T = 2.03 M_{\odot}$ White Dwarf Sequence. The variables in the lower plot are the same as Figure 8, but the simulations all are performed in the rotating reference frame with the second-order accurate FDH code. The solid curve is the stability test of the terminal model on the sequence (a = 2.53); the dashed curve is the test of the model with a = 2.63; the dot-dashed curve is the test of the model at the minimum (a = 2.67); and the triple dot-dashed curve is the test of the model just past point of contact (a = 2.80). The moments of inertia of the binary models at the points of contact, minima, and termination along the equilibrium sequence are labelled with the letters C, M, and T, respectively. For convenience, the sequence itself has been reprinted from Figure 4 in the upper plot.

Fig. 10.-Evolution of Stable Binary. Isodensity images of a stable binary with the WD equation of state, $M_T = 2.03 M_{\odot}$, and a = 2.67. The density level is 5×10^{-4} of the maximum density. Figure 10a was taken at $t = 0.0 P_I$; 10b at $t = 0.8 P_I$; 10c at $t = 1.5 P_I$; 10d at $t = 2.3 P_I$; 10e at $t = 3.0 P_I$; and 10f at $t = 3.8 P_I$. Since the simulation was performed in the rotating frame, the binary does not appear to pivot very much in this set of images.

Fig. 11.–Stability Tests of the $M_T = .500 M_{\odot}$ White Dwarf and the n = 1.5 Sequences. The same variables and code as used in Figure 9. The solid curve is the simulation of the terminal model (a = 2.45) on the $M_T = .500 M_{\odot}$ white dwarf sequence (the equilibrium sequence itself is reprinted from Figure 4 in the upper plot); the dashed curve is the test of the model on this same sequence with a = 2.63; and the dot–dashed curve is the test of the terminal model (a = 2.45) on the n = 1.5 polytropic sequence.

Fig. 12.–Stability Tests of n = 1.0 Sequence. The same variables and code as described in Figure 9. The solid curve is the test of the terminal model (a = 2.62); the dashed curve is the test of the model with a = 2.70; the dot–dashed curve is the test of the model at the minimum of the sequence (a = 2.88); and the triple dot–dashed curve is the test of the model with a = 3.28. The equilibrium sequence itself is reprinted from Figure 1 in the upper plot.

Fig. 13.–Stability Tests of n = 0.5 Sequence. The same variables and code as described in Figure 9. The solid curve is the test of the terminal model (a = 2.77); the short dashed curve is

the test of the model at the minimum of the sequence (a = 3.10); the dot-dashed curve is the test of the model with a = 3.17; the triple dot-dashed curve is the test of the model with a = 3.24; and the long dashed curve is the test of the model with a = 3.41. The equilibrium sequence itself is reprinted from Figure 1 in the upper plot.

Fig. 14.–Stability Tests of Equation of State L Sequence. The same variables and code as described in Figure 9. The solid curve is the test of the model near the minimum of the sequence (a = 2.79); the dashed curve is the test of the model with a = 3.26. The equilibrium sequence itself is reprinted from Figure 7 in the upper plot.

Fig. 15.–Stability Tests of Equation of State F Sequence. The same variables and code as described in Figure 9. The solid curve is the test of the system at the minimum of the sequence (a = 2.80). The equilibrium sequence itself is reprinted from Figure 7 in the upper plot.

Fig. 16.–White Dwarf Equilibrium Sequences. $M_T = .298, .500, .803, 1.19, 1.63, 2.03, 2.36, 2.58, 2.72, 2.81, and 2.85 M_{\odot}$.

Table 1: Lane-Emden Constants, m_n and ${r_n}^{\rm a}$

n	m_n	r_n
0.5	3.7871	2.7528
1.0	3.14159	3.14159
1.5	2.71406	3.65375

^aFrom Chandrasekhar (1967)

Table 2: Separation of Models at Minima of Polytropic Sequences

Technique, Authors	n = 0.5	n = 1.0	n = 1.5
Analytic, LRS	2.99^{a}	2.76^{a}	2.55^{a}
SPH, RS		2.90^{a}	2.67^{b}
HSCF, New & Tohline	$3.20^{\rm c}$	$2.98^{\rm c}$	$2.77^{\rm c}$
HSCF, New & Tohline	3.11^{d}	2.89^{d}	$2.70^{\rm d}$

 $^a\mathrm{From}$ LRS (1993b), separation between components' centers of mass

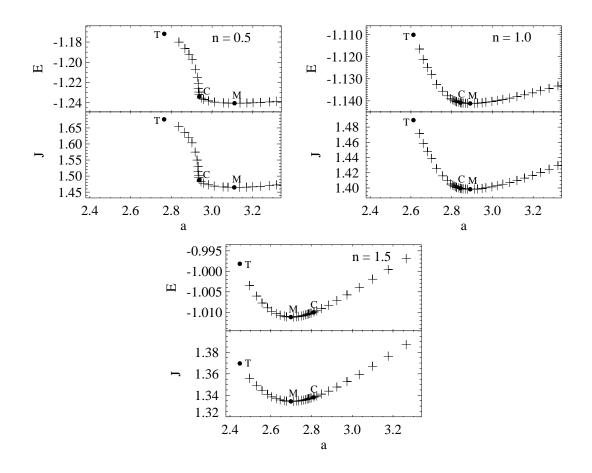
 $^b\mathrm{From}$ RS (1995), separation between components' centers of mass

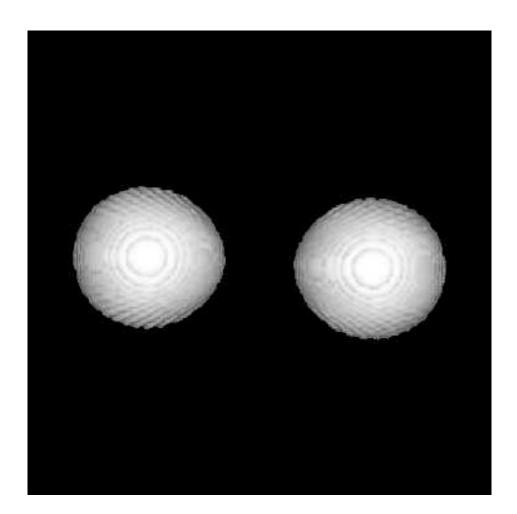
 $^c{\rm From}$ this work, separation between components' centers of mass

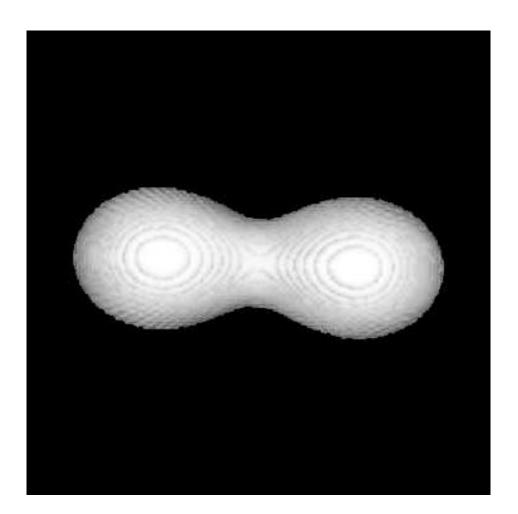
 $[^]d\mathrm{From}$ this work, separation between components' pressure maxima

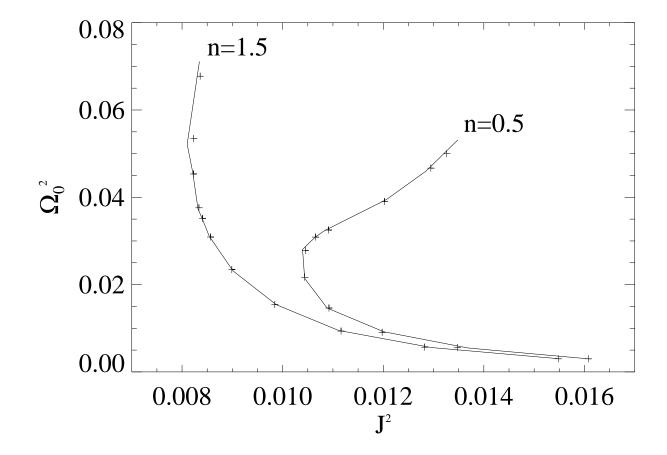
Table 3: Comparison of 64^3 and 128^3 Sequences

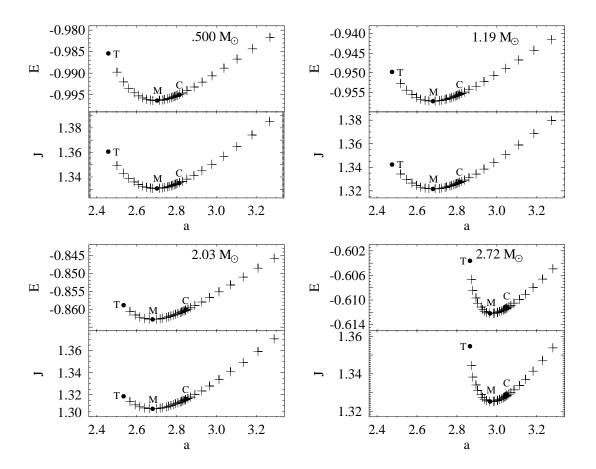
EOS, M_T	Grid Size	a(C)	a(M)	a(T)
WD, 2.03 M_{\odot}	64^{3}	2.84	2.67	2.53
	128^{3}	2.84	2.68	2.53
WD, .500 M_{\odot}	64^{3}	2.81	2.70	2.45
	128^{3}	2.81	2.70	2.46
n = 1.5	64^{3}	2.81	2.70	2.45
	128^{3}	2.81	2.70	2.45
n = 1.0	64^{3}	2.84	2.88	2.62
	128^{3}	2.84	2.89	2.61
n = 0.5	64^{3}	2.94	3.10	2.77
	128^{3}	2.94	3.11	2.76

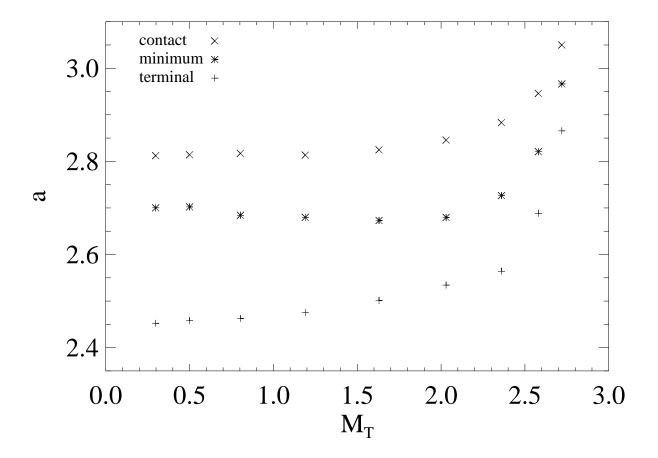


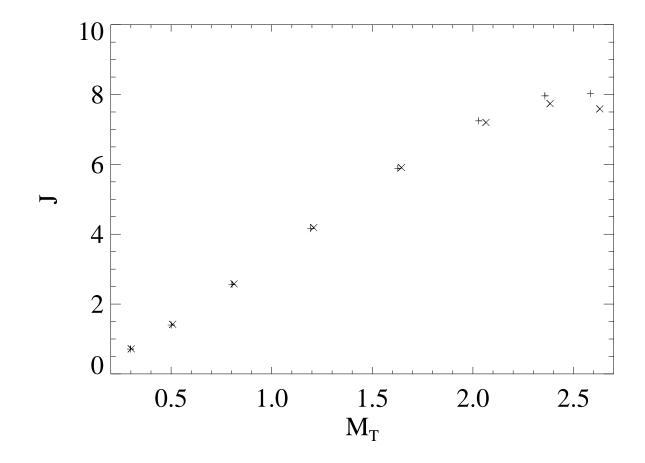


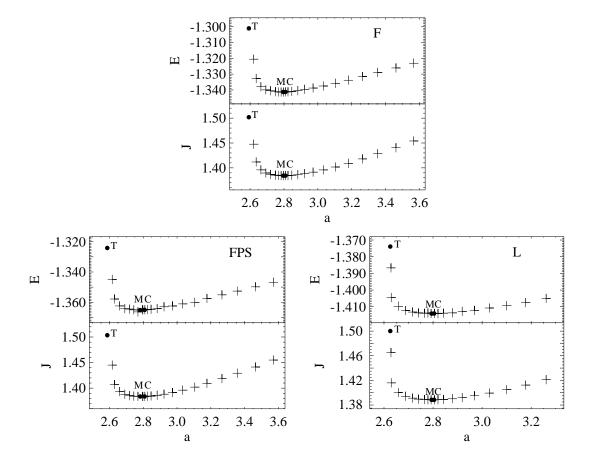


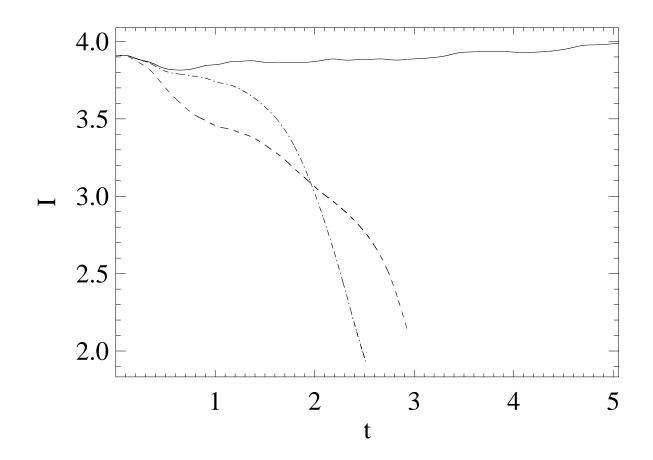


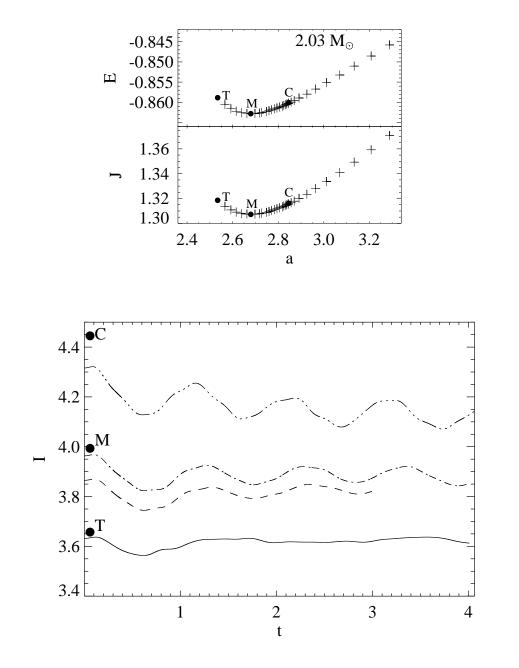


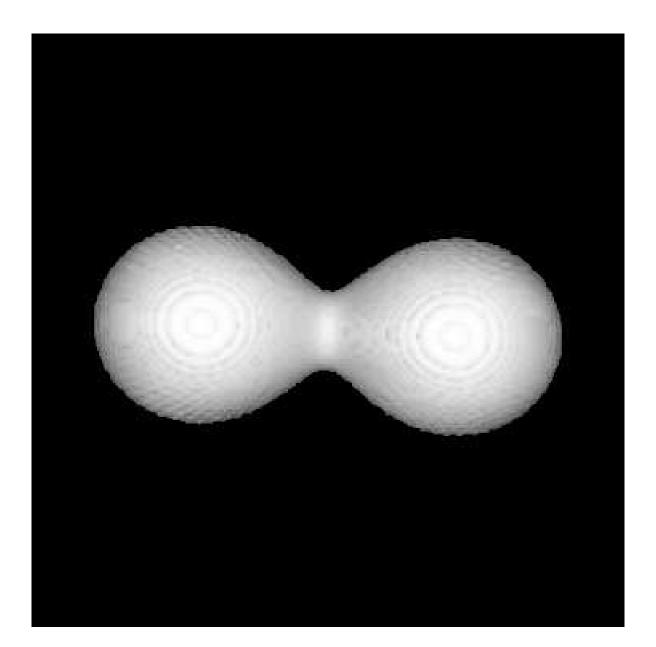


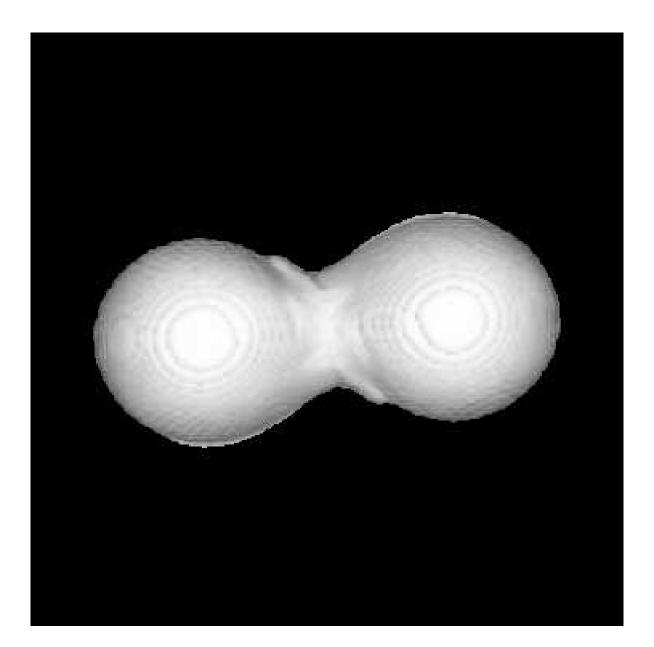


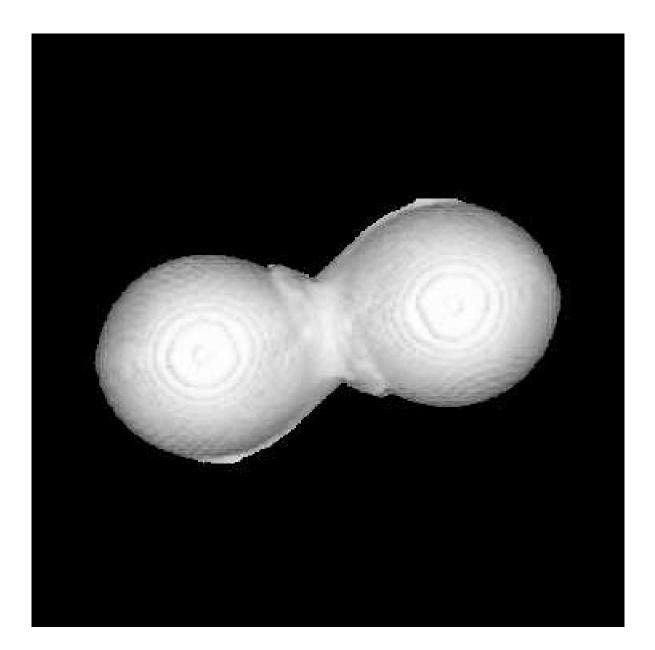


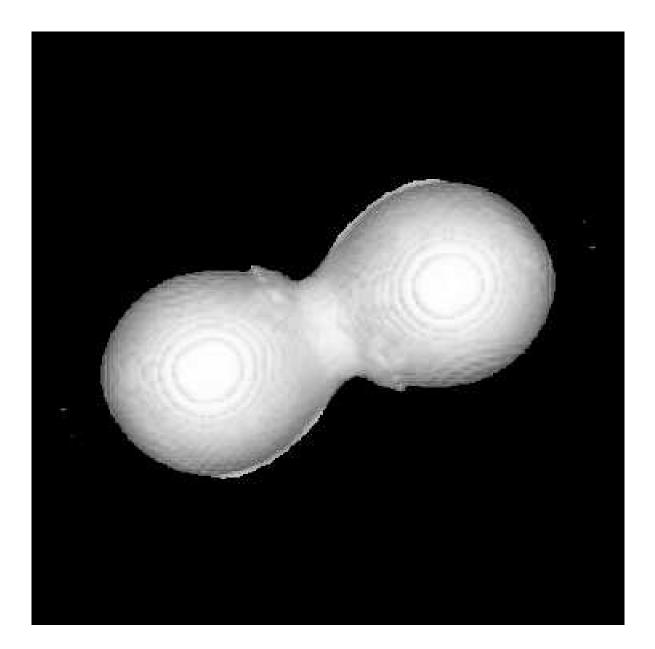


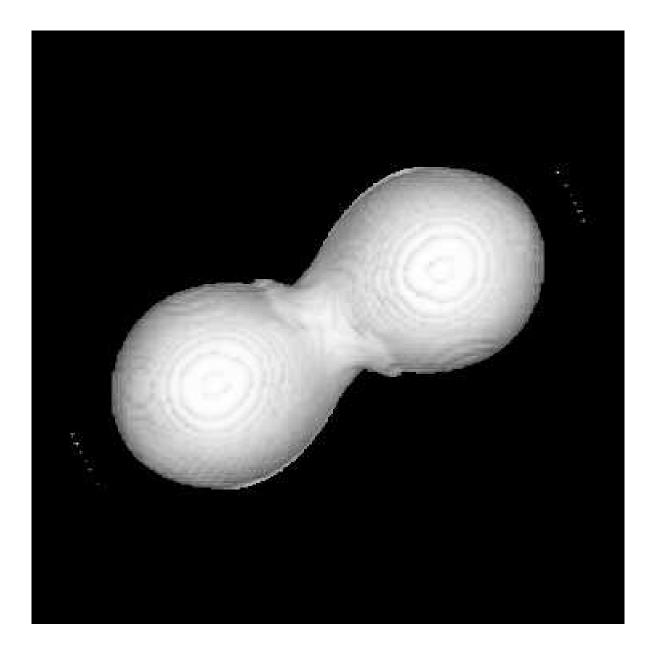


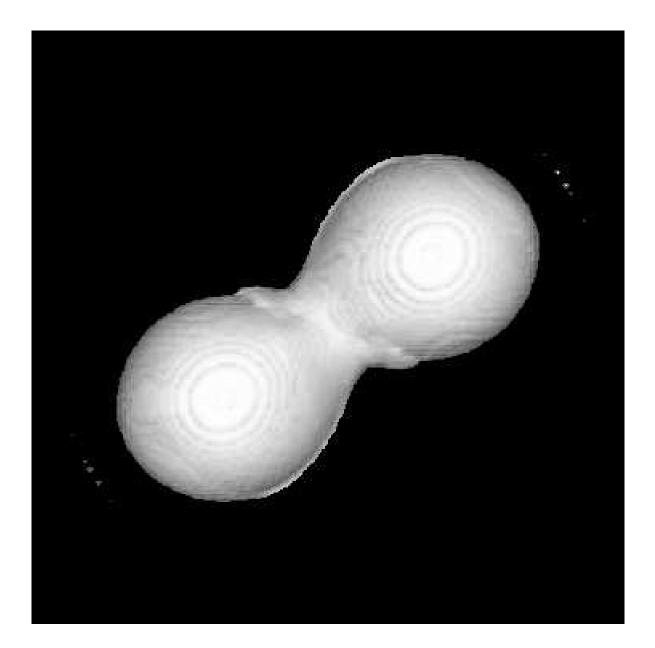


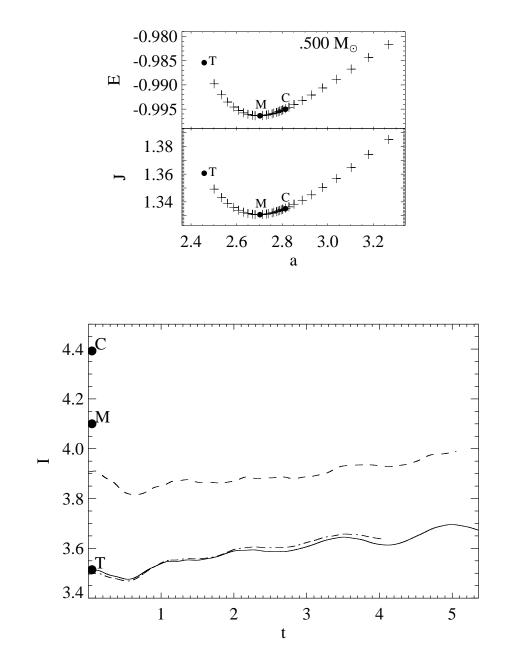


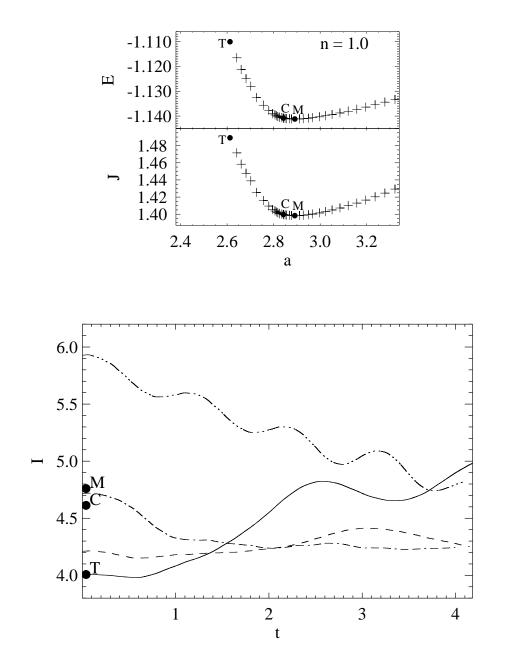


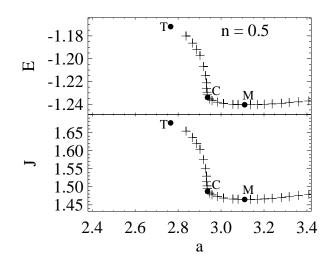


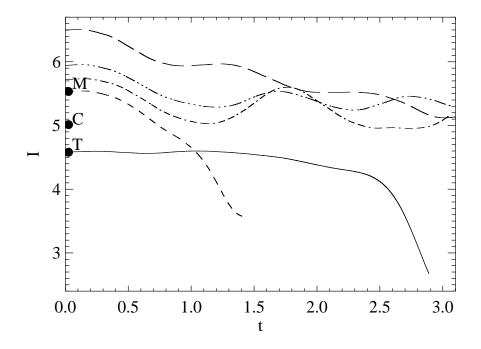


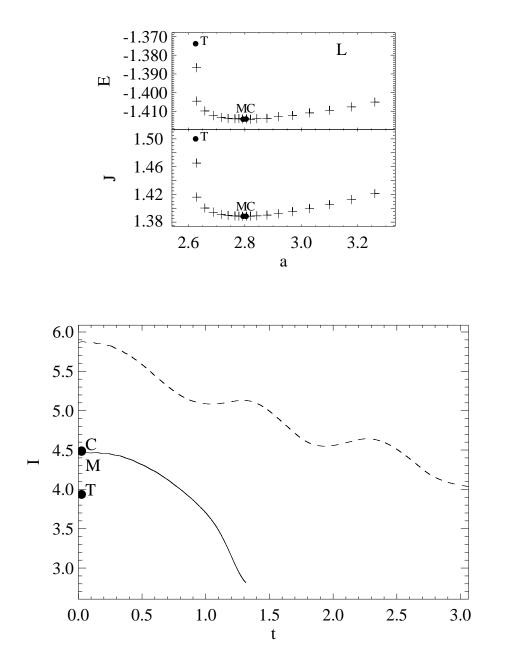


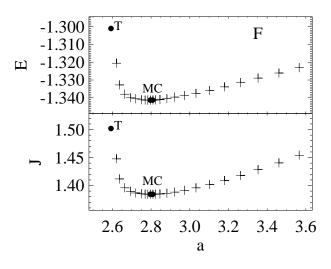


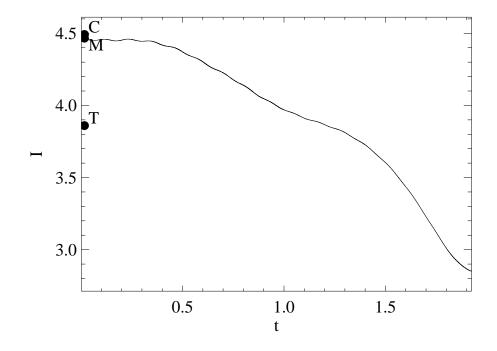


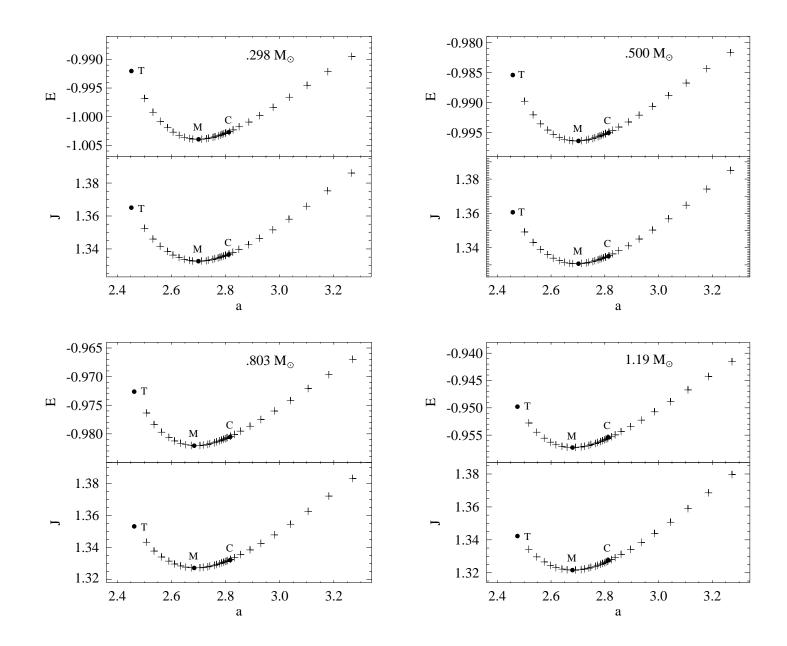




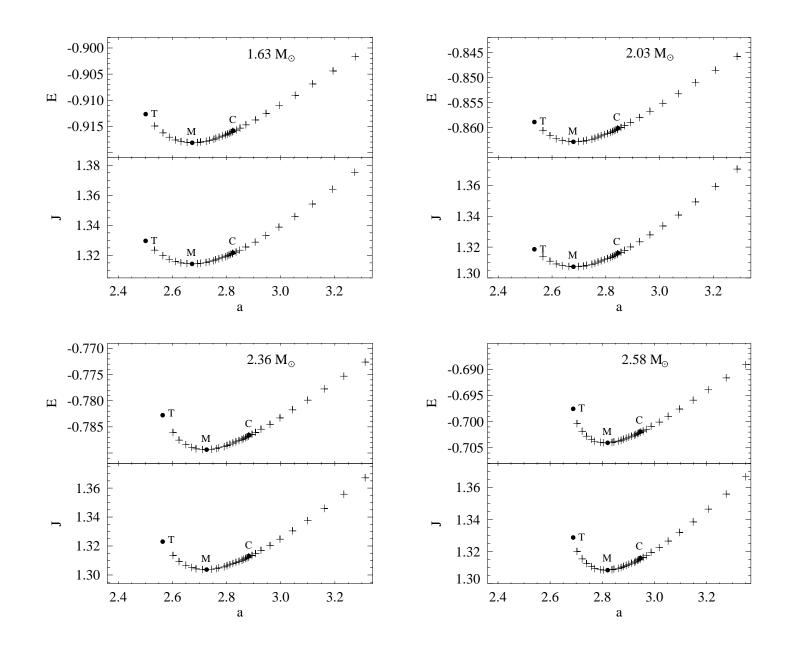




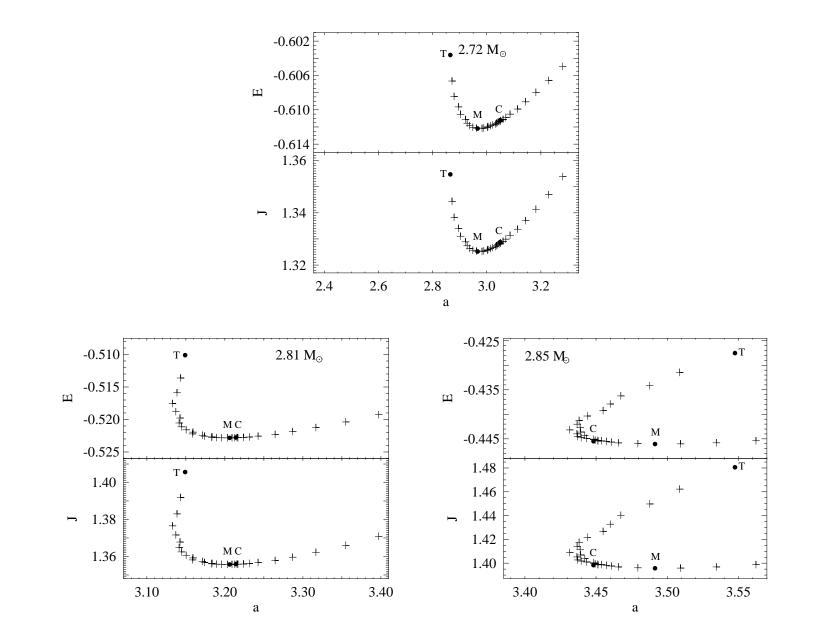




-51 -



-52 -



-53 -